communications chemistry

A Nature Portfolio journal

Article

https://doi.org/10.1038/s42004-026-02146-9

Continuous-flow photogeneration of nitrosobenzaldehydes enables indazolone formation

Check for updates

Nicolas Leclercq[1,2], Diana V. Silva-Brenes[2,3], Jean-Christophe M. Monbaliu[2,4] ✉ & Marcus Baumann[1] ✉

1,2-Dihydro-3*H*-indazol-3-ones (indazolones) are nitrogen-containing heterocycles with broad biological relevance, yet their synthesis often relies on harsh conditions or expensive metal catalysts. Herein, we report a metal-free continuous-flow photochemical protocol that enables rapid access to indazolone cores under mild and sustainable conditions. Direct irradiation of *o*-nitrobenzyl alcohols in ethanol at 365 nm generates *o*-nitrosobenzaldehydes in situ, which subsequently undergo condensation-cyclization with primary amines to afford indazolones. UV-visible spectroscopy combined with conceptual DFT analysis suggests that reaction efficiency is governed by wavelength-dependent substrate absorption: weak absorbers generate nitroso intermediates inefficiently, whereas strongly absorbing substrates undergo competitive photodegradation. By matching the irradiation wavelength to the absorption properties of individual substrates, the accessible chemical space can be extended beyond that obtained under fixed-wavelength conditions. Conceptual DFT further rationalizes substituent-dependent electronic effects, clarifying how photophysical and polar reactivity factors jointly control productive indazolone formation. The reaction scalability is assessed with commercial flow reactors.

1,2-Dihydro-3*H*-indazol-3-one derivatives (indazolones) are valuable nitrogen-containing heterocycles that have attracted sustained attention due to their diverse properties, including anti-inflammatory[1,2], anticancer[3–5], and antimicrobial activities (Fig. 1a, compounds **4-I**–**IV**)[6]. Beyond their role as pharmacophores in drug discovery, indazolones also serve as versatile building blocks in synthetic chemistry[7]. Despite this broad interest, access to libraries of functionalized indazolones remains limited as their preparation often relies on demanding or poorly generalizable methods[8].

Conventional approaches to indazolone cores typically involve cyclization or rearrangement strategies that require transition-metal catalysis[9] or harsh reaction conditions, which can compromise functional group tolerance and late-stage functionalization (Fig. 1b)[7,10–13]. Alternative photochemical protocols have been recently reported under batch conditions; however, these protocols often suffer from long irradiation times and limited efficiency, hindering their translation to larger scale (Fig. 1c)[8,14,15]. In this context, continuous-flow processing offers distinct advantages, particularly when combined with photochemistry and when reactive intermediates are involved, by enabling improved irradiation control and enhanced reproducibility (Fig. 1d)[16–22].

Herein, we report a metal-free photochemical protocol implemented under continuous-flow conditions for the rapid synthesis of indazolone scaffolds. Under controlled irradiation, readily available *o*-nitrobenzyl alcohols **1** undergo in situ photoconversion to *o*-nitrosobenzaldehydes **2**[23] (Fig. 1d, see also SI Section 1.3., Fig. S2), which subsequently react with primary amines **3** in a condensation-cyclization sequence to afford indazolones **4**. This approach leverages flow chemistry for the controlled generation and in situ consumption of reactive intermediates[24–26].

In addition to developing a synthetic protocol, we sought to rationalize its scope and limitations using spectroscopic and computational tools. UV-visible absorption spectroscopy was used to correlate substrate absorption features with productive reactivity under fixed irradiation conditions (365 nm), while conceptual density functional theory (cDFT) was used to assess how electronic substituent effects modulate the reactivity of key intermediates. Together, these complementary analyses offer mechanistic

[1]School of Chemistry, University College Dublin, Science Centre South, Belfield, Ireland. [2]Center for Integrated Technology and Organic Synthesis (CiTOS), MolSys Research Unit, University of Liège, Liège, Belgium. [3]FloW4all Flow Technology Resource Center, MolSys Research Unit, University of Liège, Liège, Belgium. [4]WEL Research Institute, Wavre, Belgium. ✉e-mail: jc.monbaliu@uliege.be; marcus.baumann@ucd.ie

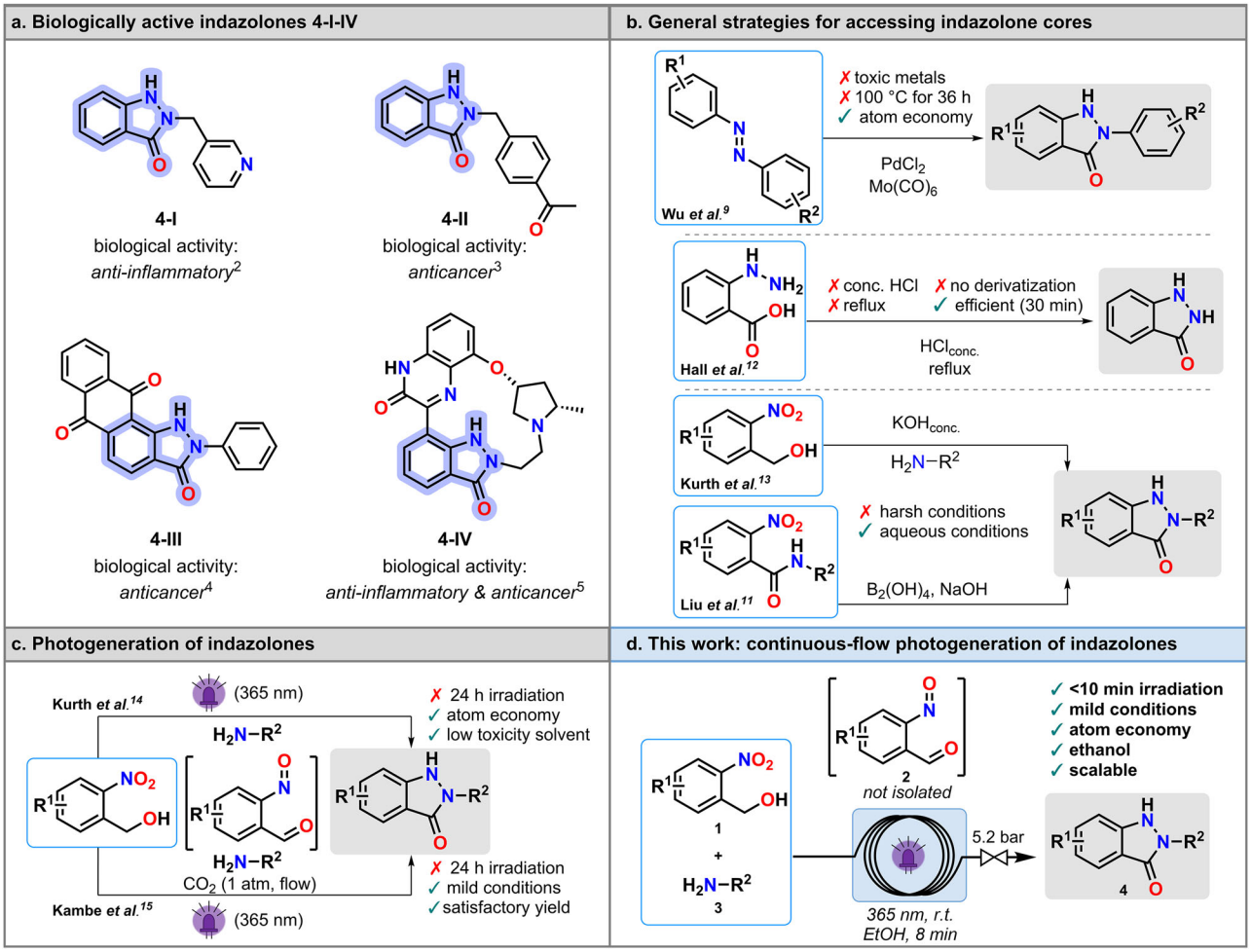


Fig. 1 | Overview of the applications and synthetic protocols targeting indazolone. a Structures of biologically active compounds containing indazolone moieties. **b** Previously reported chemical synthesis of indazolone derivatives, presenting both advantages and drawbacks for each method. **c** Previously reported photochemical methods for the synthesis of indazolone derivatives through the transient formation of o-nitrosobenzaldehyde. **d** General scheme of the work reported in this paper adapting the photochemical synthesis of indazolone derivative to a scalable, continuous-flow system.

insight into the factors governing indazolone formation and establish a rational basis for selecting effective reaction conditions. The scalability of the protocol is then demonstrated with commercial flow reactors.

Results and discussion

Reaction optimization

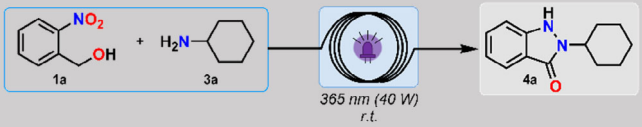
This investigation started with the batch synthesis of *N*-cyclohexylindazolone (**4a**) using conditions reported in the literature (0.5 mmol of **1a**, 2 equiv. of **3a**, 365 nm irradiation at 3 ×18 W for 24 h), reported to afford **4a** in 71% yield[10]. Following this precedent, a mixture of *o*-nitrobenzyl alcohol (**1a**, 1 equiv.) and cyclohexylamine (**3a**, 2 equiv.) was initially prepared in a phosphate-buffered saline (PBS). However, the limited solubility of **1a** resulted in precipitation, thus preventing direct translation to continuous-flow conditions. To address this limitation, a 70:30 (v/v) PBS/ethanol mixture was employed, affording complete dissolution of both reagents. The resulting solution was processed in a commercial lab-scale flow reactor (Vapourtec E-Series) equipped with a 365 nm UV lamp (See SI, Scheme S1). Using an initial residence time of 10 min and a lamp power of 40 Watt, indazolone **4a** was obtained in 70% yield by qNMR, with incomplete conversion of **1a** accounting for the remaining material (Table 1, Entry 1).

A brief solvent screening was then conducted to improve reaction efficiency. Increasing the ionic strength of the buffer proved detrimental (Table 1, Entry 2), while replacing PBS with non-buffered medium led to a slightly decreased yield (Table 1, Entry 3). In contrast, performing the reaction in pure ethanol resulted in near-complete conversion with high selectivity (Table 1, Entry 4). On this basis, subsequent optimization studies were conducted in ethanol. Reaction parameters were next examined using a one-factor-at-a-time approach. Increasing the concentration of **1a** led to a reduced conversion and lower yield (Table 2, Entry 2-3), while decreasing the residence below 8 min resulted in incomplete conversion (Table 2, Entries 7-8). In contrast, reducing the residence time from 10 to 8 minutes had no measurable impact on the yield (Table 2, Entry 6). Next, reducing the excess amine **3a** to 1.2 equiv. had no adverse effect (Table 2, Entries 4-5). The influence of lamp power was also evaluated. Reducing the power to 20 Watt decreased the yield, whereas increasing it to 80 Watt gave complete conversion (Table 2, Entries, 9-10). Measurements of the molar absorption coefficients at 365 nm indicated that product **4a** (ε_{365} = 365 L.mol^{-1}.cm^{-1}) absorbs more strongly than starting alcohol **1a** (ε_{365} = 172 L.mol^{-1}.cm^{-1}), indicating that a substantial proportion of the incident photons is absorbed by the product[27]. While higher lamp power marginally improved conversion, excessive irradiation was therefore avoided to minimize competing secondary photochemical processes, especially for halogenated substrates. Based on these results, the following conditions were selected for subsequent studies, unless otherwise stated: 50 mM substrate in ethanol, 1.2 equiv. of amine, a residence time of 8 min, and irradiation of 365 nm with a lamp power of 40 W (Table 2, Entry 12).

Extension of the scope with substituted aryl derivatives 1a-h

Using the optimized photo-flow conditions established for model alcohol **1a**, a series of substituted *o*-nitrobenzyl alcohols (**1b**-**h**) was evaluated with

Table 1 | Scope of solvents



Entry	Concentration of 1a (mM)	Solvent	Amine (equiv.)	Lamp Power (W)	Residence Time (min)	Conversion of 1a (%)[a]	qNMR Yield (%)[a]
1	50	PBS/EtOH	2	40	10	70	70
2	50	Conc. PBS/EtOH	2	40	10	60	51
3	50	Water/EtOH (1:1)	2	40	10	70	66
4	50	EtOH	2	40	10	97	94

[a]Conversion and yield were calculated using trimethoxybenzene as internal standard in ^{1}H qNMR experiments.

Table 2 | Optimization of reaction conditions



Entry	Concentration of 1a (mM)	Solvent	Amine (equiv.)	Lamp Power (W)	Residence Time (min)	Conversion of 1a (%)[a]	qNMR Yield (%)[a]
1	50	EtOH	2	40	10	97	94
2	100	EtOH	2	40	10	77	73
3	150	EtOH	2	40	10	63	62
4	50	EtOH	1.5	40	10	98	88
5	50	EtOH	1.2	40	10	98	88
6	50	EtOH	2	40	8	93	93
7	50	EtOH	2	40	5	86	84
8	50	EtOH	2	40	2	61	61
9	50	EtOH	2	20	10	84	83
10	50	EtOH	2	80	10	>98	95
11	50	EtOH	2	0	10	4	0
12	50	EtOH	1.2	40	8	>98	96 (96)[b]

[a]Conversion and yield were calculated using trimethoxybenzene as internal standard in ^{1}H qNMR experiments.
[b]Isolated yield.

cyclohexylamine (**3a**) under continuous -low conditions. Under these conditions, a small library of indazolones (**4b**-**4h**) was obtained with yields ranging from low to high, depending on the nature of the aryl substitution pattern (Fig. 2). Good performances were observed for substrates **1a, 1b, 1d, 1f**-**h**, whereas no indazolone formation was detected with derivatives **1c** and **1e**. For several substrates (notably, **1c, 1e, 1f**) extensive degradation was observed, with little to no recovery of the starting *o*-nitrobenzyl alcohol. Additionally, dehalogenation was detected for halogenated compounds **4g** and **4h**. To determine whether this photoreduction originated from the starting *o*-nitrobenzyl alcohol or from the indazolone product, both **1h** and

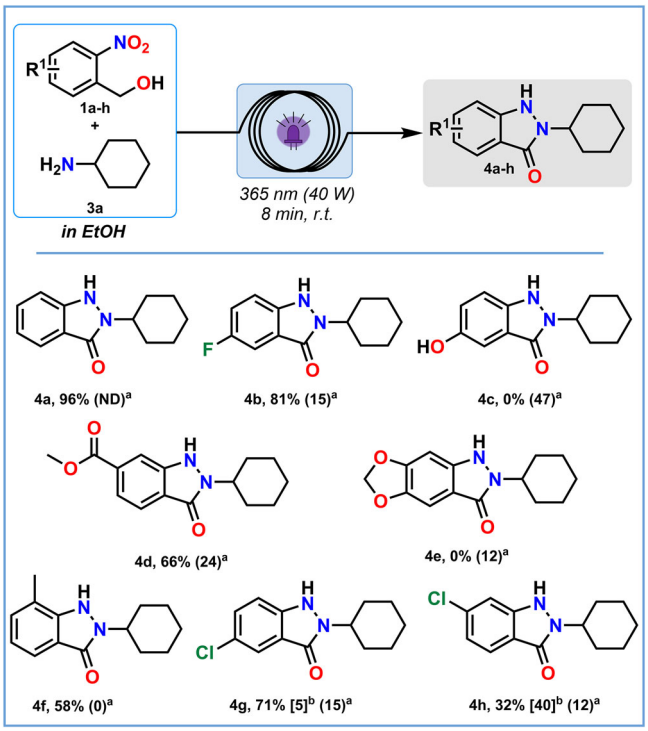


Fig. 2 | Indazolone substrate scope. Reaction conditions: a feed solution containing **1** (1.0 mmol) and **3a** (1.2 equiv.) in EtOH was irradiated under UV light (365 nm, 40 W) at 25 °C for 8 min of residence time. ^{1}H-NMR yields were calculated using trimethoxybenzene as an internal standard. [a]Yields reported in parentheses correspond to unreacted starting *o*-nitrobenzyl alcohol (**1**) derivative. [b]Yields reported in square brackets refer to the dehalogenated side product formed from chlorine-containing derivatives, affording **4a**.

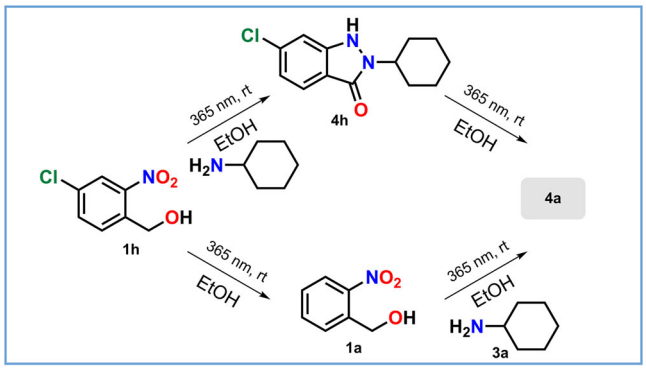


Fig. 3 | Proposed pathways for the observed reduction of 4h into 4a. Top: photochemical synthesis of indazolone **4h**, followed by subsequent dehalogenation to afford **4a**. Bottom: initial dehalogenation of *o*-nitrobenzyl alcohol **1h** to form **1a**, followed by reaction with **3a**, leading to production of **4a**.

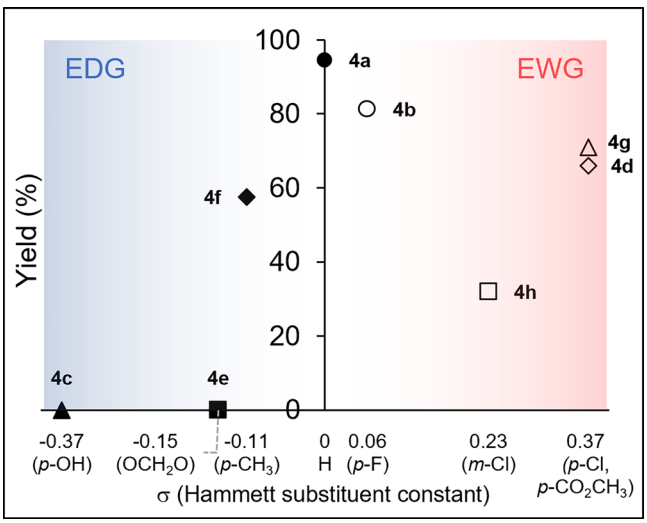


Fig. 4 | Yield (%) of indazolone versus Hammett sigma constants of the substituents. NMR yields were calculated using trimethoxybenzene as an internal standard.

isolated **4h** were independently subjected to the optimized reaction conditions (Table 2, Entry 12). These control experiments revealed that **4h** undergoes selective photodehalogenation, with 34% conversion to **4a**, indicating that formation of **4a** arises predominantly from the degradation of the product rather than the starting material (**1h**, Fig. 3).

To assess the influence of electromodulating substituents on productive indazolone formation, the yields obtained from substrates **1a-h** were plotted against the corresponding Hammett σ substituent constants (Fig. 4). The use of Hammett σ values allows to rank the electron withdrawing or donating properties of the substituents used[28], thus enabling comparison of substituent effects on conversion. Because the substituents concomitantly affect multiple parameters in photochemical process (e.g. absorption wavelength, degradation pathways), these correlations are interpreted qualitatively rather than as true kinetic parameters. Overall, Fig. 4 indicates that the transformation tolerates electron-withdrawing (EWG) and electron-neutral substituents, whereas substrates bearing strong electron-donating groups (EDG) fail to afford the desired indazolones. Halogenated compound **4h** is a notable outlier due to partial dehalogenation into **4a**.

Aside from modulating the electron structure of the aromatic ring, substituents influence the absorption features of the substrate and, consequently, the efficiency of photochemical nitroso generation. To evaluate this effect, UV-visible absorption spectra were taken for all investigated *o*-nitrobenzyl alcohols (See SI Section 1.2., Fig. S1). Consistent with the established photophysical trends, EWG substituents induce hypsochromic shifts, whereas EDG substituents induce bathochromic shifts. Plotting the normalized absorbance at the experimental irradiation wavelength (365 nm) against Hammett σ constants confirms that EDG-substituted substrates, such as **1c** and **1e**, have absorption maxima that are closer to this wavelength than their EWG counterparts (See SI Section 1.4., Fig. S3). We hypothesize that excessive absorption promotes competing photochemical pathways, leading to substrate degradation. Our results indeed show a correlation between low indazolone yield and substrates with absorption maxima near 365 nm (See SI Section 1.4., Fig. S4). On the EWG side of the Hammett scale, diminished absorption limits productive nitroso photogeneration, thus resulting in incomplete conversion and recovery of starting material. Substrates lacking strong EDG or EWG substituents such as **1a** (R = H) and the fluorinated derivative **1b** display a favorable balance between sufficient absorption and photostability, making them particularly well suited for this transformation. Finally, the anomalously low yield observed for compound **4h** is attributed to competing photodehalogenation (Fig. 3), which such chlorinated derivatives are prone to undergo.

Impact of the irradiation wavelength

Guided by the structure-absorption-photoreactivity relationships established above, we next examined whether adjusting the irradiation wavelength could mitigate photodegradation while maintaining productive nitroso photogeneration. Substrate **1e** was selected as proof-of concept, as only extensive substrate degradation was observed at 365 nm (Fig. 2). The UV-visible absorption spectrum of **1e** shows a steep decrease in absorbance at wavelengths above 365 nm (See SI Section 1.2., Fig. S1). Consistent with this observation, increasing the wavelength to 400 nm enabled the formation of indazolone **4e**, albeit in modest yields (Table 3, Entry 3). Further red-

shifting of the irradiation wavelength resulted in progressively lower conversion and yield (Table 3, Entries 4-5). Across this series, an overall reduction in substrate degradation was observed while the wavelength increased, supporting the notion that wavelength tuning can partially decouple productive excitation from unproductive, competing photochemical pathways.

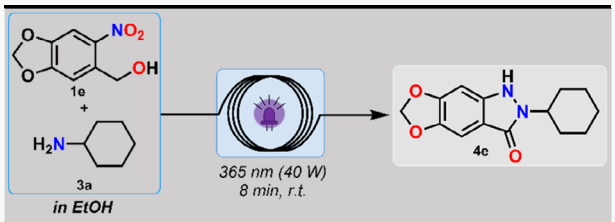
Conceptual density functional theory (CDFT) analysis

To further elucidate how electronic substituent effects influence the reactivity of the nitroso intermediates, a conceptual Density Functional Theory (cDFT) analysis was performed on *o*-nitrosobenzaldehyde intermediates (**2a-h**) derived from substrates **1a-h**. Global and local electrophilicity indices as well as electrostatic potential (ESP) maps were computed[29]. Details are listed in the Supporting Information (See SI, Section 2.1.).

Electrostatic Surface Potential (ESP) maps of the optimized intermediates reveal two distinct electrophilic regions corresponding to the nitroso and aldehyde moieties, respectively (Fig. 5). Local electronic descriptors (See SI, Section 2.2.) show that the nitroso moiety (ω_N) is consistently more electrophilic than the aldehyde group (ω_C), supporting nucleophilic attack at the nitroso nitrogen as the dominant pathway. A strong correlation between the ω_N and Brown's substituent constants (σ_p^+, See SI, Figure S8) highlights even more the strong electrophilicity of the nitroso moiety, which can be described as having a pseudo-cationic character. A second observation concerns the magnitude of the effect exerted by aryl substitution on both reactive centers. The local electrophilicity at the nitroso center varies significantly with aryl substitution ($0.94 < \omega_N < 1.18$), whereas the aldehyde carbon displays much smaller variations ($0.07 < \omega_C < 0.12$). The fact that NO is the most reactive center and also the most sensitive to modulation is reflected in the large yield variations observed with different substituents.

The combined use of UV-visible spectroscopy and cDFT analysis provides a global description of the factors governing indazolone formation under photochemical conditions. Efficient reaction requires sufficient substrate absorption at the irradiation wavelength to enable nitroso generation, while avoiding excessive absorption that promotes degradation. For strongly electron-rich substrates, photodegradation resulting from excessive absorption precedes and dominates over polar reactivity considerations, whereas for less strongly donating systems, electrophilicity becomes the limiting factor. Once the nitroso intermediate is formed, its electrophilicity, which is modulated by aryl substitution, controls its ability to undergo nucleophilic attack by amine **3**, thereby determining productive indazolone formation.

Table 3 | Scope of wavelengths



Entry	Wavelength (nm)	Conversion of 1e (%)[a]	qNMR yield (%)[a]
1	365	88	ND
2	385	77	ND
3	400	58	15
4	425	40	5
5	450	16	ND

[a]^{1}H-NMR yields were calculated using trimethoxybenzene as an internal standard. Yields in parentheses are unreacted starting *o*-nitrobenzyl alcohol **1e**.

Scope of amines

With optimized reaction conditions in hand, the substrate scope was next extended by varying amine coupling partner **3** (Table 2, Entry 12). Diversification was explored using *o*-nitrobenzyl alcohols **1a,b** (Fig. 6), selected on the basis of their reliable performances under optimized conditions, with **1b** additionally chosen due to the relevance of fluorinated cores in medicinal chemistry.

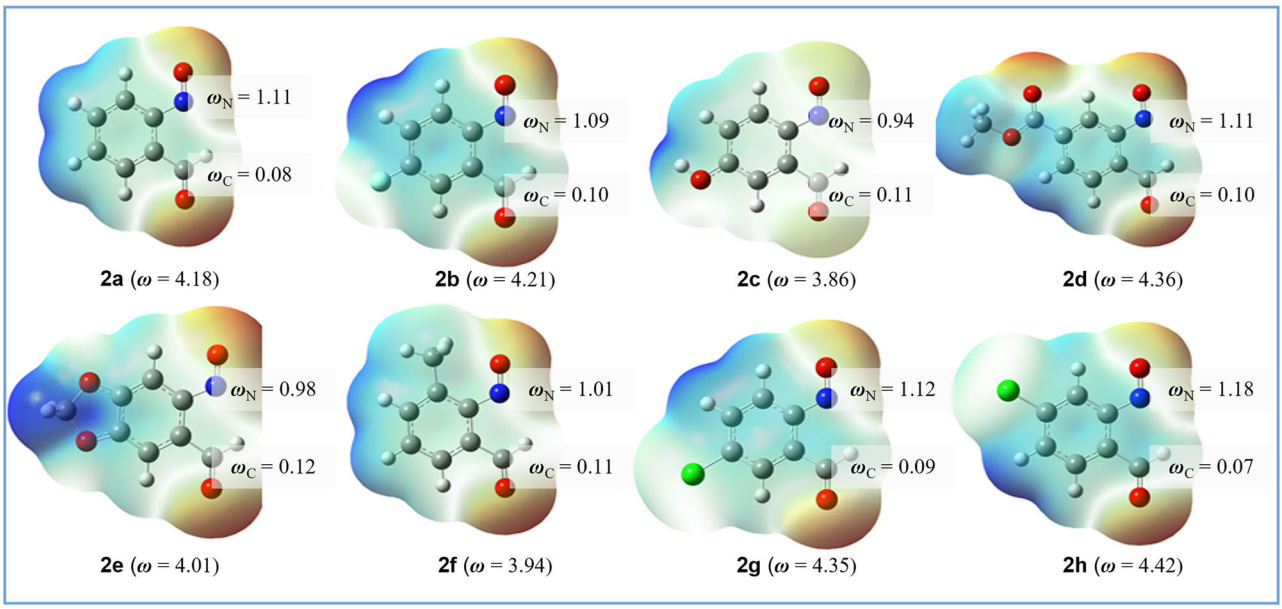


Fig. 5 | Electrostatic potential (ESP) surface plots of the intermediate *o*–nitrosobenzaldehydes 2. Regions of negative electrostatic potential (electron-rich) are indicated in red, while regions of positive electrostatic potential (electron-deficient) are highlighted in blue. The local electrophilicity indexes at the nitroso nitrogen (ω_N) and of the aldehyde carbon (ω_C), as well as the global electrophilicity index (ω) are reported for each structure.

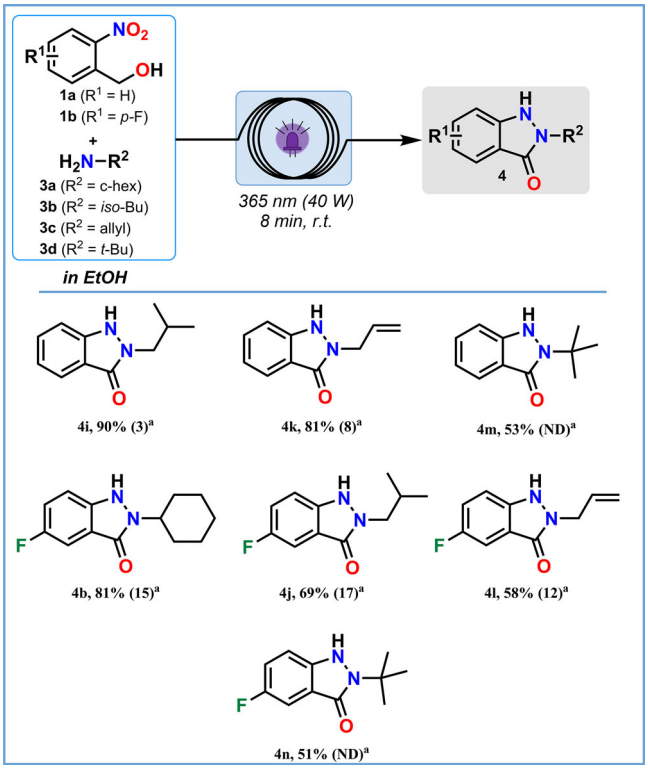


Fig. 6 | Indazolone amine scope. Reaction conditions: a feed solution containing **1** (1.0 mmol) and **3** (1.2 equiv.) in EtOH was irradiated under UV light (365 nm, 40 Watt) at 25 °C for 8 min of residence time. ^{1}H-NMR yields were calculated using trimethoxybenzene as an internal standard. [a]Yields reported in parentheses correspond to unreacted starting *o*-nitrobenzyl alcohol (**1**) derivative.

All tested alkyl amines gave the corresponding indazolones in moderate to excellent yields. Fluorinated derivatives consistently afforded lower yields. This decrease in efficiency may stem from the reaction conditions, which were specifically optimized for the unsubstituted *o*-nitrobenzyl alcohol derivative.

Long run and scalability assessment

In order to assess the temporal stability of the reaction, a long run experiment was carried out under the optimized conditions (Table 2, Entry 12). The reaction was monitored every hour *via* ^{1}H qNMR analysis. Over more than 6 h of continuous reaction, 3.60 g of **4a** was isolated (86.2% isolated yield), while the conversion and yield, determined by qNMR, remained stable at 95% and 91%, respectively (Fig. 7a). For such long runs, a decrease in yield was observed when using denatured ethanol. GC-MS analysis of the feed solution suggested that this deterioration arises from slow reaction of cyclohexamine (**3a**) with 2-butanone used as denaturant.

In addition, the scalability of the process was evaluated by transposing it to a Corning® Advanced-Flow™ Lab Photo Reactor. By decreasing the residence time to 1 min 22 s, a space-time yield (STY) of up to 409.6 $g.L^{-1}.h^{-1}$ was achieved, while maintaining both conversion and yield above 90% (Fig. 7b). For comparison, the Vapourtec setup under the optimized conditions (Table 2, Entry 12) afforded a STY of 77.8 $g.L^{-1}.h^{-1}$, whereas the same photochemical reaction reported by Kurth et al. displayed an STY of 0.32 $g.L^{-1}.h^{-1}$ [14]. More importantly, the scalability of reactions performed in Corning® Advanced-Flow™ Reactor technology is well established up to industrial scale, ensuring transposition of these conditions to production scales[30,31].

Given that the two flow photochemical setups led to markedly different outcomes, and since lamp power had previously been identified as a key parameter influencing the reaction behavior, actinometric measurements were performed in order to quantify the effective photon flux delivered by each reactor. Solutions of *(E)*-azobenzene (80 mM) were passed through the reactors and irradiated at 365 nm under varying lamp intensities. The *(E)* → *(Z)* photoisomerization was monitored through ^{1}H NMR spectroscopy. Due to fast reaction kinetics, the lamps could not be operated at full power. However, plotting the measured conversion *versus* the light power revealed a linear relationship, indicating that the photon flux increased proportionally with the lamp power for both photoreactors (See SI, Section 2.1.). By extrapolating our data and by using the 0.12 quantum yield of the isomerization at 365 nm already reported in a similar research case[32], the photon fluxes could be calculated. Based on our experiments, the Vapourtec R-Series reactor at 40 W and the Corning® Advanced-Flow™ Lab Photo Reactor at 100% power are estimated to have photon fluxes of 2.57×10^{-5} and 3.74×10^{-5} mol photons·s^{-1}, respectively. The higher space-time yield reached in the Corning® Lab Photo Reactor can be partly rationalized by its higher photon flux, which irradiates a reduced reactor volume compared to the Vapourtec equipment, combined with superior mass-transfer (mixing) of Corning reactors.

Conclusion

This project successfully demonstrated the synthesis of indazolone derivatives *via* a metal-free photochemical strategy operating in ethanol under short residence times and conducted under continuous-flow conditions. By leveraging the in situ generation of reactive *o*-nitrosobenzaldehydes from *o*-nitrobenzyl alcohols under 365 nm LED irradiation, followed by cyclization with primary amines, various nitrogen-containing heterocycles were obtained in modest to excellent yields. Beyond reducing reaction times, the continuous-flow format proved essential for controlling photon flux, maintaining steady-state conditions over extended operation, and enabling transposition of reaction conditions between photoreactor platforms. These aspects are difficult to decouple or systematically optimize under batch conditions, particularly for reactions involving short-lived nitroso intermediates.

Electron-poor and electron-neutral substrates proved well suited to the optimized conditions, while electron-rich *o*-nitrobenzyl alcohols failed to generate the desired indazolone products. Electron-donating substituents led to extensive decomposition of the starting material, which may arise from the high absorptivity of these compounds at 365 nm. UV-Vis analysis indicated that irradiation at longer wavelengths (400–425 nm) enables activation of an electron-rich substrate (**1e**) while decreasing decomposition by selecting an irradiation wavelength where the substrate sufficiently absorbs light to trigger the reaction without promoting unwanted secondary reactions. In general, the results were rationalized by comparing the absorption maxima (λ_{max}) of the substrates; however, a more rigorous understanding would require quantitative comparison of their molar absorptivities (ε). Although not explored in this work, energy-transfer photocatalysis remains an attractive alternative to decouple excitation from substrate absorption, which may in turn result in better conversion while minimizing substrate degradation. Complementary DFT analysis further explains this poor yield as a consequence of the low electrophilicity of the intermediate, hindering the subsequent nucleophilic attack by the amine.

Overall, this work highlights how modern synthetic chemistry, through the synergy of photochemistry, flow processing, and theoretical insight, can offer both efficiency and sustainability in the development of green and readily scalable routes.

Methods

General methods

Optimization of continuous-flow reactions were carried out on a Vapourtec E-Series system equipped with peristaltic pumps and a static back-pressure regulator (75 psi, 5.2 bar). The long run and actinometry tests were performed in a Vapourtec R-Series system equipped with high-pressure piston pumps and a static back pressure regulator (75 psi, 5.2 bar). For photochemical experiments, the UV-150 module from Vapourtec was mainly used in combination with a high-power double-sided LED (365 nm, purchased from Vapourtec) regulated between 20 W and 80 W. The system was

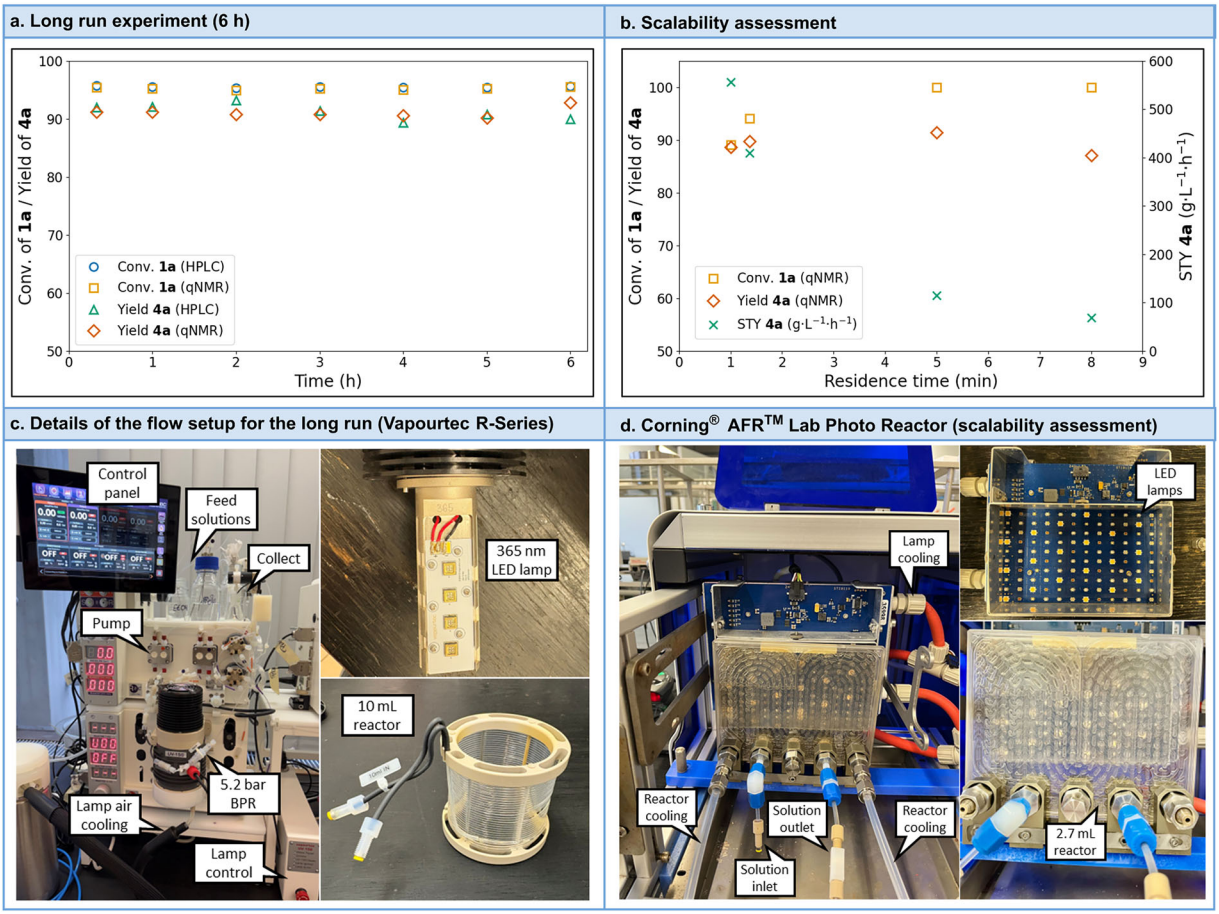


Fig. 7 | Long run and scalability assessment. a Conversion and yield for the photochemical synthesis of **4a** using the optimized continuous-flow conditions over a total run time of 400 min. The reaction was performed on a Vapourtec R-Series reactor equipped with a photochemical module, and monitored by ^{1}H qNMR using trimethoxybenzene as an internal standard and HPLC using anisole as an internal standard. **b** Conversion, yield and space-time yield (STY) as a function of residence time following transposition of the reaction to a Corning® Advanced-Flow™ (AFR) Lab Photo Reactor. Conversion and yield were determined by ^{1}H qNMR using trimethoxybenzene as internal standard. **c** Overall view of the Vapourtec R-series setup, highlighting the main system components. **d** Overall view of the Corning® Lab Photo Reactor, highlighting the LED panel and the glass fluidic module (2.7 mL internal volume).

cooled to 23–28 °C by passing a stream of compressed air through the reactor unit. No optical filters were used. A 20 mm distance separated the lamp from the reactor. The coil was placed inside the reactor that included a reflecting medium, guaranteeing efficient irradiation. Reactor coils were made of perfluoroalkoxy polymer (PFA) tubing with a 1/16-inch external diameter (1 mm internal diameter) and a volume of 10 mL.

Additional UV light sources used for the synthesis of **4e** are either single-sided UV lamps with a wavelength of 385 nm, 400 nm, or 425 nm, or a double-sided UV lamp of 450 nm. All lamps were purchased from Vapourtec. All single-sided lamp powers were set at 40 W. The double-sided 450 nm lamp had a fixed power of 54 W.

The scalability assessment for the continuous-flow synthesis of **4a** was carried out in a Corning® Advanced-Flow™ (AFR) Lab Photo Reactor system equipped with 2 LED panels. An 18 mm distance separated both lamps from the reaction plate. The reactor used was a Corning glass plate with 2.7 mL of internal volume. The LED panels were cooled around 25 °C using a thermostat using a 1:1 mixture of ethanol and water as heat transfer fluids. A second thermostat was used to control the reaction temperature by circulating a 7 wt% ethylene glycol in water solution through the service channels of the Corning Lab Reactor module. The reaction feed solution was pumped using an Asia Syringe Pump equipped with two syringes of 2.5 mL and 5.0 mL, respectively.

Unless otherwise stated, all solvents were purchased from Fisher Scientific or Sigma-Aldrich and used without further purification. Similarly, unless specified otherwise, all reagents were obtained from Fluorochem, Sigma-Aldrich, or TCI. Reagent quality was assessed by NMR analysis prior to use, and all materials were employed as received.

General procedure used for optimization of the synthesis of indazolone derivatives 4

To a 50 mL volumetric flask, 20 mL of non-denatured ethanol, 2-nitrobenzyl alcohol **1** (2.5 mmol, 1 equiv.) and amine derivatives **3** (3 mmol, 1.2–1.5 equiv.) were added. The volume was completed using ethanol. The reaction solution was passed through a Vapourtec E-Series reactor (10 mL of internal volume) at a flow rate of 1.25 mL.min^{-1} (8 min of residence time). The solution was irradiated within the flow reactor by a 40 W 365 nm UV lamp. After waiting 20 min (2.5 residence time) for the reaction to reach steady-state, the solution was collected for 16 min (20 mL, 1 mmol of product expected). The collected solution was washed with 1 M HCl and extracted using dichloromethane. The organic layers were dried using anhydrous sodium sulfate, filtered, and concentrated under vacuum. Then the crude reaction mixture was purified by chromatography on silica and eluted with a gradient of dichloromethane/methanol or cyclohexane/ethyl acetate (based on TLC tests) to obtain the desired product.

Long run synthesis of 4a

To a 500 mL volumetric flask, 200 mL of non-denatured ethanol, 2-nitrobenzyl alcohol **1a** (3.84 g, 25.11 mmol, 1 equiv.) and cyclohexylamine **3a** (3.11 g, 31.47 mmol, 1.2 equiv.) was added. The volume was completed using ethanol. The reaction solution was passed through a

Vapourtec R-Series reactor (10 mL of internal volume) at a flow rate of 1.25 mL.min^{-1} (8 min of residence time). The solution was illuminated within the flow reactor by a 40 W 365 nm UV lamp. Samples were taken every hour and analyzed through ^{1}H qNMR. The collected solution (385.2 mL, rest was used for analysis) was washed with 1 M HCl and extracted using dichloromethane. The organic layers were dried using sodium sulfate, filtered, and concentrated under vacuum. Then, the crude reaction mixture was purified by chromatography on silica and eluted with a gradient of dichloromethane/ethanol (dichloromethane → dichloromethane/ethanol 4:1). After drying, 4.74 g (16.67 mmol, 86.2% yield) of the title compound was obtained as a dark oil. For details, see SI section **1.5**.

Proof-of-scalability in the Corning® lab photo reactor

To a 100 mL volumetric flask, 50 mL of non-denatured ethanol, 2-nitrobenzyl alcohol **1a** (741 mg, 4.84 mmol, 1 equiv.) and cyclohexylamine **3a** (596 mg, 6.01 mmol, 1.2 equiv.) was added. The volume was completed using ethanol. The reaction solution was passed through the Corning AFR reactor (2.7 mL of internal volume) at a flow rate of 0.338 to 2.7 mL.min^{-1} (0.5 to 4 min of residence time). The solution was illuminated within the flow reactor by two 9.2 W 365 nm UV lamps (100% power). The collected solution was washed with 1 M HCl and extracted using dichloromethane. The organic layers were dried using sodium sulfate, filtered, and concentrated under vacuum. For details, see SI section **1.6**.

Data availability

The authors declare that the main data supporting the findings of this study, including experimental procedures and compound characterization, NMR, and HRMS are available within the article and its Supplementary Information file or from the corresponding author on reasonable request.

Received: 29 October 2025; Accepted: 14 July 2026;
Published online: 14 August 2026

References

1. Tse, E., Butner, L., Huang, Y. & Hall, I. H. The anti-inflammatory activity of N-substituted indazolones in mice. *Arch. Pharm.* **329**, 35–40 (1996).
2. Bruneau, P., Delvare, C., Edwards, M. P. & McMillan, R. M. Indazolinones, a new series of redox-active 5-lipoxygenase inhibitors with built-in selectivity and oral activity. *J. Med. Chem.* **34**, 1028–1036 (1991).
3. Hall, I. H., Wong, O. T., Hall, E. S. & Chen, L. K. The Cytotoxicity of N-substituted indazolones in murine and human tumor cells. *Anticancer Drugs* **4**, 389–393 (1993).
4. Wang, H., Han, H. & Von Hoff, D. D. Identification of an agent selectively targeting DPC4 (deleted in pancreatic cancer locus 4)-deficient pancreatic cancer cells. *Cancer Res.* **66**, 9722–9730 (2006).
5. Kawanishi, N. et al. Structure-based drug design of a highly potent CDK1,2,4,6 inhibitor with novel macrocyclic quinoxalin-2-one structure. *Bioorg. Med. Chem. Lett.* **16**, 5122–5126 (2006).
6. Roth, A. et al. Inhibition of myeloperoxidase: evaluation of 2H-indazoles and 1H-indazolones. *Bioorg. Med. Chem.* **22**, 6422–6429 (2014).
7. Muthumani, P., Meera, R. & Devi, P. Synthesis and biological study of some novel Schiff's bases of indazolone derivatives. *J. Chem. Pharm. Res* **2**, 433–443 (2010).
8. Nie, H. J., Guo, A., Di, Lin, H. X. & Chen, X. H. Rapid and halide compatible synthesis of 2-*N*-substituted indazolone derivatives via photochemical cyclization in aqueous media. *RSC Adv.* **9**, 13249–13253 (2019).
9. Wang, Z., Yin, Z., Zhu, F., Li, Y. & Wu, X.-F. Palladium-catalyzed carbonylative cyclization of azoarenes. *ChemCatChem* **9**, 3637–3640 (2017).
10. Zhu, J. S. et al. N-N Bond formation between primary amines and nitrosos: direct synthesis of 2-substituted indazolones with mechanistic insights. *Org. Lett.* **20**, 4736–4739 (2018).
11. Bao, Y. et al. A B2(OH)4-mediated synthesis of 2-substituted indazolone and its application in a DNA-encoded library. *Org. Lett.* **22**, 6277–6282 (2020).
12. Wyrick, S. D., Joseé Voorstad, P., Cocolas, G. & Hall, I. H. Hypolipidemic activity of phthalimide derivatives. 7. Structure-activity studies of indazolone analogues. *J. Med. Chem.* **27**, 768–772 (1984).
13. Oakdale, J. S., Solano, D. M., Fettinger, J. C., Haddadln, M. J. & Kurth, M. J. An oxazolo[3,2-b]indazole route to 1H-Indazolones. *Org. Lett.* **11**, 2760–2763 (2009).
14. Zhu, J. S., Kraemer, N., Li, C. J., Haddadin, M. J. & Kurth, M. J. Photochemical preparation of 1,2-dihydro-3-H-indazol-3-ones in aqueous solvent at room temperature. *J. Org. Chem.* **83**, 15493–15498 (2018).
15. Yang, T. et al. Photocatalyst-free synthesis of indazolones under CO_2 atmosphere. *Chem. Asian J.* **14**, 1436–1442 (2019).
16. Gérardy, R. et al. Continuous flow organic chemistry: successes and pitfalls at the interface with current societal challenges. *Eur. J. Org. Chem.* **2018**, 2301–2351 (2018).
17. Capaldo, L., Wen, Z. & Noël, T. A field guide to flow chemistry for synthetic organic chemists. *Chem. Sci.* **14**, 4230–4247 (2023).
18. Monbaliu, J.-C. M. & Legros, J. Will the next generation of chemical plants be in miniaturized flow reactors?. *Lab Chip* **23**, 1349–1357 (2023).
19. Crawford, R. & Baumann, M. Continuous flow technology enabling photochemistry. *Adv. Synth. Catal.* **367**, e202500133 (2025).
20. Teixeira, R. I. et al. Scale-up of continuous metallaphotoredox catalyzed C-O coupling to a 10 kg-scale using small footprint photochemical Taylor vortex flow reactors. *Org. Process Res. Dev.* **29**, 34–47 (2025).
21. Buglioni, L., Raymenants, F., Slattery, A., Zondag, S. D. A. & Noël, T. Technological innovations in photochemistry for organic synthesis: flow chemistry, high-throughput experimentation, scale-up, and photoelectrochemistry. *Chem. Rev.* **122**, 2752–2906 (2022).
22. Bonciolini, S., Pulcinella, A. & Noël, T. Tech-enhanced synthesis: exploring the synergy between organic chemistry and technology. *J. Am. Chem. Soc.* **147**, 28523–28545 (2025).
23. Spennacchio, M., Natho, P., Andresini, M. & Colella, M. Continuous flow generation of highly reactive organometallic intermediates: a recent update. *J. Flow. Chem.* **14**, 43–84 (2024).
24. Jamieson, P., Cronly, D. & Baumann, M. Generation and use of reactive intermediates exploiting flow technology. *Chimia* **79**, 396–403 (2025).
25. Dallinger, D., Gutmann, B. & Kappe, C. O. The concept of chemical generators: on-site on-demand production of hazardous reagents in continuous flow. *Acc. Chem. Res.* **53**, 1330–1341 (2020).
26. Klán, P. et al. Photoremovable protecting groups in chemistry and biology: reaction mechanisms and efficacy. *Chem. Rev.* **113**, 119–191 (2013).
27. Bonfield, H. E. et al. Photons as a 21st century reagent. *Nat. Commun.* **11**, 804–807 (2020).
28. Hansch, C., Leo, A. & Taft, R. W. A Survey of Hammett substituent constants and resonance and field parameters. *Chem. Rev.* **91**, 165–195 (1991).
29. Domingo, L. R., Ríos-Gutiérrez, M. & Pérez, P. Applications of the conceptual density functional theory indices to organic chemistry reactivity. *Molecules* **21**, 748 (2016).
30. Steiner, A. et al. Multikilogram per hour continuous photochemical benzylic brominations applying a smart dimensioning scale-up strategy. *Org. Process. Res. Dev.* **24**, 2208–2216 (2020).
31. Bianchi, P., Petit, G. & Monbaliu, J.-C. M. Scalable and robust photochemical process towards small spherical gold nanoparticles. *React. Chem. Ing.* **5**, 1224–1236 (2020).
32. Roseau, M., Chausset-Boissarie, L., Gremetz, S., Roth, P. M. C. & Penhoat, M. Multiple wavelength (365–475 nm) complete actinometric characterization of Corning® Lab Photo Reactor using

azobenzene as a highly soluble, cheap and robust chemical actinometer. *Photochem. Photobiol. Sci.* **21**, 421–432 (2022).

Acknowledgements

The School of Chemistry at UCD is acknowledged for providing access to spectroscopic facilities including NMR spectroscopy (Dr Yannick Ortin and Dr Patricia Fleming) and mass spectrometry (Dr Jimmy Muldoon).

Author contributions

Nicolas Leclercq: Experimental Work, Writing—original draft. Diana V. Silva-Brenes: Supervision, Writing—review and editing. Jean-Christophe M. Monbaliu: Conceptualization, Project Administration, Supervision, Funding Acquisition, Writing—review and editing. Marcus Baumann: Conceptualization, Project Administration, Supervision, Funding Acquisition, Writing—review and editing.

Funding

The authors acknowledge the Erasmus+ Programme of the European Union under grant agreement B LIEGE01 (mobility allowances for Nicolas Leclercq). The authors acknowledge the “Fonds de la Recherche Scientifique” (F.R.S.-FNRS) for funding. Computational resources were provided by the “Consortium des Équipements de Calcul Intensif” (CÉCI), funded by the “Fonds de la Recherche Scientifique de Belgique” (F.R.S.-FNRS) under Grant No. 2.5020.11a. The manuscript was written through contributions of all authors. All authors have given approval to the final version of the manuscript.

Competing interests

The authors declare no competing interests.

Additional information

Supplementary information The online version contains supplementary material available at https://doi.org/10.1038/s42004-026-02146-9.

Correspondence and requests for materials should be addressed to Jean-Christophe M. Monbaliu or Marcus Baumann.

Peer review information *Communications Chemistry* thanks the anonymous reviewers for their contribution to the peer review of this work.

Reprints and permissions information is available at http://www.nature.com/reprints

Publisher’s note Springer Nature remains neutral with regard to jurisdictional claims in published maps and institutional affiliations.

Open Access This article is licensed under a Creative Commons Attribution-NonCommercial-NoDerivatives 4.0 International License, which permits any non-commercial use, sharing, distribution and reproduction in any medium or format, as long as you give appropriate credit to the original author(s) and the source, provide a link to the Creative Commons licence, and indicate if you modified the licensed material. You do not have permission under this licence to share adapted material derived from this article or parts of it. The images or other third party material in this article are included in the article’s Creative Commons licence, unless indicated otherwise in a credit line to the material. If material is not included in the article’s Creative Commons licence and your intended use is not permitted by statutory regulation or exceeds the permitted use, you will need to obtain permission directly from the copyright holder. To view a copy of this licence, visit http://creativecommons.org/licenses/by-nc-nd/4.0/.

© The Author(s) 2026